Journal of Fluids and Structures (1997) **11,** 395–412

A NEW TWIST ON AN OLD MODEL FOR VORTEX-EXCITED VIBRATIONS

R. A. SKOP AND S. BALASUBRAMANIAN
Division of Applied Marine Physics
Rosenstiel School of Marine and Atmospheric Science, University of Miami
Miami, FL 33149, U.S.A.

(Received 27 May 1996 and in revised form 22 January 1997)

A new twist on an old model for predicting the vortex-excited vibrations of flexible cylindrical structures is developed. A van der Pol equation, driven by the local transverse motion of the cylinder, is taken as the governing equation for one component of the fluctuating lift force on the cylinder. The second component of the lift force is represented by a stall term which is linearly proportional to the local transverse velocity of the cylinder. In previous models, the van der Pol equation has been employed as the governing equation for the entire fluctuating lift force on the cylinder. The new model preserves the modal scaling principle for the structural response, as initially predicted by the previous models and since verified experimentally. The empirical parameters in the model are related to the physical mass and damping parameters that define the structural properties so that the maximum structural response and the reduced velocity at which it occurs agree with experimental observations. Because of the stall term, the new model provides for an asymptotic, self-limiting structural response at zero structural damping. This asymptotic, self-limiting behavior was not captured by the previous models.

1. INTRODUCTION

THE PERIODIC SHEDDING OF VORTICES that accompanies cross-flow past a bluff cylindrical body can excite the body into resonant transverse vibrations when the vortex-shedding frequency and a body's natural frequency are sufficiently close to one another. About two decades ago, several investigators began employing nonlinear oscillator equations of the van der Pol type to represent the fluctuating lift force on the cylinder (Hartlen & Currie 1970, Skop & Griffin 1973, Iwan & Blevins 1974, Skop & Griffin 1975, Iwan 1975). This representation for the lift force was based more on the similarity between the vortex-shedding process and the behavior of nonlinear oscillators than on the underlying fluid dynamics. The models, however, did succeed in identifying the reduced damping as the controlling factor in determining the structural response (Skop & Griffin 1973, Iwan & Blevins 1974). The reduced damping is defined, essentially, by the ratio of the structural damping to the ratio of the fluid to structural masses. The models also succeeded in identifying the modal scaling principle for the structural response (Skop & Griffin 1975, Iwan 1975). The modal scaling principle collapses the responses of different-type structures to vortex shedding to a single curve through a mode shape factor.

Numerous variations of the original nonlinear oscillator models have since been proposed. Updated reviews can be found in Parkinson (1989) and Billah (1989). These variations, for the most part, have concentrated on the response of spring-mounted

0889–9746/97/040395 + 18 $25.00/fl970085

circular cylinders to vortex shedding with an eye towards portraying some of the more subtle details of the response not described by the original models (for example, the occasionally observed hysteretic response behavior). The variations have met with only limited success in reproducing these subtle details. Moreover, the variations, also for the most part, have sacrificed the modal scaling principle of the original models; a fact usually not noted in review articles.

None of the models, to date, have accurately captured the asymptotic, self-limiting structural response near zero structural damping (Griffin *et al.* 1982). This response is characterized by a maximum, peak-to-peak vibratory amplitude of about two cylinder diameters. Further, the response is asymptotic in that the maximum amplitude varies little for a range of small structural damping values.

Recently, Albarède & Monkewitz (1992) have demonstrated that the nonlinear oscillator equations arise as the leading order approximation for the vortex shedding instability from a stationary cylinder. The leading order nature of these equations explains, perhaps, not only the success of the nonlinear oscillator models in predicting much of the structural response behavior to vortex shedding, but also their failure to reproduce the subtle details of the response.

In light of the more thorough grounding of their fluid dynamical origins and limitations, it is appropriate to revisit the nonlinear oscillator models to clarify the nature of the asymptotic, self-limiting structural response near zero structural damping. We do so here. Specifically, we take a van der Pol equation to represent the behavior of one component of the fluctuating lift force on a cylindrical structure. This component of the lift force is driven by the transverse motion of the structure. The second component of the lift force is represented by a stall term. This term is taken as linearly proportional to the transverse velocity of the structure. The appearance of a stall component, and its form, in the overall fluctuating lift force has been suggested by Triantafyllou *et al.* (1994) based on their examination of lift measurements on mechanically oscillated cylinders. The inclusion of the stall term in our model provides for the appropriate asymptotic, self-limiting structural response at zero structural damping. The empirical parameters in the model are developed in terms of the mass and damping parameters that define the structural properties, so as to establish congruence between the predicted maximum structural response and the reduced velocity at which it occurs, and experimental observations. The new model preserves both the dependence of the structural response on the reduced damping and the modal scaling principle for the structural response.

2. MODEL EQUATIONS AND MODAL SCALING

Consider a flexible, circular cylindrical structure subjected to a uniform cross-flow of velocity V of a fluid having density ρ. The structure is characterized by its diameter D and total length L. The measure of length along the structure is denoted by x. The vortex-induced fluctuating lift force caused by the flow forces the structure into motion in a direction transverse to the flow. The amplitude of this motion, normalized by the structural diameter D, is given by $Y(x, t)$, where t denotes time.

To formulate the model for determining $Y(x, t)$, it is useful to adopt a normal mode approach. Hence, $Y(x, t)$ is developed as

$$Y(x, t) = \sum_i y_i(t)\psi_i(x), \tag{1}$$

where $\psi_i(x)$ is the ith normal mode of the structure and $y_i(t)$ is the modal response

factor. The dynamical equations for the $y_i(t)$ are obtained as [see, for example, Thomson (1965)]

$$\int_0^L \psi_i^2(x)\,\mathrm{d}x\{\ddot{y}_i + 2\zeta_i\omega_{n,i}\dot{y}_i + \omega_{n,i}^2 y_i\} = \frac{\rho V^2}{2(m_s + m_a)}\int_0^L C_L(x,t)\psi_i(x)\,\mathrm{d}x, \tag{2}$$

where a dot implies differentiation with respect to time. In equation (2), m_s is the structural mass per unit length of the structure, m_a is fluid added mass per unit length of the structure, $\omega_{n,i}$ is the *in situ* natural frequency of the structure in the ith vibrational mode, and ζ_i is the corrected structural damping ratio in the ith vibrational mode. The corrected structural damping ratio is defined by

$$\zeta_i = \zeta_{s,i}\sqrt{\frac{m_s}{m_s + m_a}}, \tag{3}$$

where $\zeta_{s,i}$ is the actual structural damping ratio in the ith mode as measured, in practice, in air. Previous investigators have interpreted ζ_i in equation (2) as the actual structural damping. This interpretation is mathematically consistent for a structure in air, but the corrected value given by equation (3) must be used for similar mathematical consistency in other circumstances.

The coefficient of fluctuating lift, denoted by $C_L(x, t)$, is constructed as

$$C_L(x,t) = Q(x,t) - \frac{2\alpha}{\omega_s}\dot{Y}(x,t). \tag{4}$$

Here, α is a parameter to be evaluated from experimental results and ω_s is the intrinsic vortex-shedding frequency determined from the Strouhal relation

$$\omega_s = \frac{2\pi SV}{D}, \tag{5}$$

where S is the Strouhal number. The second term on the right-hand side of equation (4) provides that the magnitude of the fluctuating lift force has a negative slope for large structural motions and, in this sense, is called the stall term. The inclusion of the stall term in the fluctuating lift coefficient has, as noted, been suggested by Triantafyllou *et al.* (1994), based on evidence of this negative slope in lift measurements on mechanically oscillated cylinders. The excitation component of the fluctuating lift coefficient, represented by $Q(x, t)$, is taken to satisfy a van der Pol equation

$$\ddot{Q} - \omega_S G(C_{L0}^2 - 4Q^2)\dot{Q} + \omega_S^2 Q = \omega_S F\dot{Y}, \tag{6}$$

where C_{L0}, G and F are parameters again to be evaluated from experimental results. For flow over a stationary structure (that is, for $\dot{Y} = 0$), equation (6) has a self-excited, self-limited solution,

$$Q = C_{\mathrm{L0}}\sin\omega_S t. \tag{7}$$

This result leads to the definition of C_{L0} as the amplitude of the fluctuating lift coefficient on a stationary cylinder. The derivation of equation (7) requires that $C_{L0}^2 \ll 1$. Data summarized by Protos *et al.* (1968) indicates that this requirement is satisfied for cylindrical sections studied thus far.

When $\dot{Y}(x, t)$ is not constrained to be zero, the solution for $Q(x, t)$ is also sought as a modal expansion. Some simplifications can, however, be made at this point. First, Ramberg & Griffin (1974, 1976) have made measurements on vortex shedding behind a mechanically oscillated cable and have demonstrated that the near-wake properties at any point along the cable correspond to the near wake behind a rigid cylinder oscillating at the same conditions of frequency and local amplitude. That is, the near-wake properties varied modally in the same manner as the cable vibrational amplitude. Based on this experimental evidence, we assume that the modal expansion for $Q(x, t)$ contains the same normal modes as the modal expansion for $Y(x, t)$. Next, under this assumption, Skop & Griffin (1975) and Iwan (1975) have shown that the only significant contribution to the modal expansion of $Q(x, t)$ is the ith mode when ω_S is in the vicinity of one of the $\omega_{n,i}$. That is, for $\omega_S \approx \omega_{n,i}$, $Q(x, t)$ can be taken as

$$Q(x, t) = q_i(t)\psi_i(x), \tag{8}$$

where $q_i(t)$ is the modal response factor for the excitation component of the fluctuating lift. Substitution of the modal expansions for $Y(x, t)$ and $Q(x, t)$, equations (1) and (8), respectively, into equation (4), yields the fluctuating lift coefficient as

$$C_L(x, t) = \left[q_i(t) - \frac{2\alpha}{\omega_S}\dot{y}_i(t) \right]\psi_i(x) - \frac{2\alpha}{\omega_S}\sum_{j\neq i}\dot{y}_j(t)\psi_j(x). \tag{9}$$

On substituting this expression into equation (2), it is easy to deduce that the only forced modal component of $Y(x, t)$ is the ith component. Hence, for $\omega_S \approx \omega_{n,i}$, the modal expansion for $Y(x, t)$ reduces to

$$Y(x, t) = y_i(t)\psi_i(x), \tag{10}$$

where the response factor $y_i(t)$ satisfies the dynamical equation

$$\ddot{y}_i + 2\zeta_i\omega_{n,i}\dot{y}_i + \omega_{n,i}^2 y_i = \mu\omega_s^2\left(q_i - \frac{2\alpha}{\omega_S}\dot{y}_i \right). \tag{11}$$

In obtaining equation (11) from equation (2), the flow velocity V in equation (2) has been replaced in terms of ω_S from equation (5). The mass ratio parameter μ is defined by

$$\mu = \frac{\rho D^2}{8\pi^2 S^2(m_S + m_a)}. \tag{12}$$

The dynamical equation for $q_i(t)$ is determined by substituting equations (8) and (10) into equation (6) and applying standard modal techniques. The resulting equation is

$$\ddot{q}_i - \omega_S G C_{L0}^2\dot{q}_i + \omega_S^2 q_i + \frac{4\omega_S G}{\Gamma_i} q_i^2\dot{q}_i = \omega_S F\dot{y}_i, \tag{13}$$

where the modal factor Γ_i is given by

$$\Gamma_i = \left[\int_0^L \psi_i^2(x)\,\mathrm{d}x \right] \Big/ \left[\int_0^L \psi_i^4(x)\,\mathrm{d}x \right]. \tag{14}$$

Let us now rewrite $y_i(t)$ and $q_i(t)$ as

$$y_i(t) = \Gamma_i^{1/2} y(t), \qquad q_i(t) = \Gamma_i^{1/2} q(t). \tag{15, 16}$$

On substituting these expressions into equations (11) and (13), the governing equations for $y(t)$ and $q(t)$ are obtained as

$$\ddot{y} + 2\zeta_i \omega_{n,i} \dot{y} + \omega_{n,i}^2 y = \mu \omega_S^2 \left(q - \frac{2\alpha}{\omega_S} \dot{y} \right), \tag{17}$$

$$\ddot{q} - \omega_S G (C_{L0}^2 - 4q^2) \dot{q} + \omega_S^2 q = \omega_S F \dot{y}. \tag{18}$$

Equations (17) and (18) are independent of the ith structural mode shape and, for this reason, $y(t)$ and $q(t)$ are termed the modally independent response factors. The solutions for $y(t)$ and $q(t)$ depend only on the damping ratio ζ_i, the mass ratio μ, the natural frequency $\omega_{n,i}$ and the Strouhal frequency ω_S. The normalized amplitude of the structural motion $Y(x, t)$ and the excitation component of the fluctuating lift coefficient $Q(x, t)$ become, on substituting equation (15) into equation (10) and equation (16) into equation (8),

$$Y(x, t) = \Gamma_i^{1/2} \psi_i(x) y(t), \tag{19}$$

$$Q(x, t) = \Gamma_i^{1/2} \psi_i(x) q(t). \tag{20}$$

As should be required, $Y(x, t)$ and $Q(x, t)$ are independent of the normalization of the normal modes. That is, if $\psi_i(x)$ is scaled by a constant C, then, from equation (14), $\Gamma_i^{1/2}$ is scaled by C^{-1} so that $\Gamma_i^{1/2} \psi_i(x)$ remains unchanged. A tabulation of normal modes and modal factors for various structures can be found in Skop & Griffin (1975). As a consequence of the modal independence of $y(t)$ and $q(t)$, the quantities $Y(x, t)/[\Gamma_i^{1/2} \psi_i(x)]$ and $Q(x, t)/[\Gamma_i^{1/2} \psi_i(x)]$ also depend only on ζ_i, μ, $\omega_{n,i}$ and ω_S, which is the modal scaling principle enunciated by Skop & Griffin (1975) and Iwan (1975).

Over the years, issues have been raised concerning the appropriateness of the linear proportionality of the driving function to $\dot{Y}(x, t)$ on the right-hand side of equation (6). These issues are summarized by Billah (1989), who also suggests that the driving function should be parametric in character; that is, it should contain a multiplicative $Q(x, t)$ term. The linear proportionality to $\dot{Y}$ is based on truncating the power series expansion of a generalized forcing function $f(\dot{Y}, Q)$ at its first-order level. More complicated forms of, or terms in, the driving function, of the general nature $Q^a \dot{Y}^b$, are certainly permissible. The inclusion of such terms in equation (6) would lead to additional terms, having the construct

$$q_i^a \dot{y}_i^b \left[\int_0^L \psi_i^{a+b+1}(x)\, \mathrm{d}x \right] \Big/ \left[\int_0^L \psi_i^2(x)\, \mathrm{d}x \right],$$

on the right-hand side of equation (13). For the modal scaling principle to hold, these additional terms must scale identically with the nonlinear term $q_i^2 \dot{q}_i / \Gamma_i$ appearing on the left-hand side of equation (13). Hence, preservation of the modal scaling principle requires that the exponents a and b satisfy $a + b = 3$. Skop & Balasubramanian (1995a) recently studied mechanically oscillated cylinders using equation (6), but with a parametric driving function of the nature $Q\dot{Y}^b$. They found that a value $b = 0{\cdot}68$, not $b = 2$ as required to preserve modal scaling, was necessary to match the lock-in

boundaries measured experimentally by Williamson & Roshko (1988). As a consequence, we retain the linear driving function here as adequate for describing to first order the feedback from the oscillating structure to the fluid.

3. MODEL SOLUTIONS AND THEIR CHARACTERISTICS

We seek steady state solutions to equations (17) and (18) as

$$y = A \sin \omega t, \tag{21}$$

$$q = BC_{L0} \sin(\omega t + \varphi). \tag{22}$$

Here, ω is the joint response, or entrainment, frequency and the condition $\omega \approx \omega_S \approx \omega_{n,i}$ is implied; A and B are, respectively, amplification factors for the modally independent structural displacement and the modally independent excitation component of the fluctuating lift; and φ is the phase of the modally independent excitation component of the fluctuating lift relative to the modally independent structural displacement. On substituting equations (21) and (22) into equations (17) and (18), the joint, or entrained, response is found to be

$$A = \frac{BC_{L0}}{(S_G + \alpha)} \frac{1}{(\delta^2 + 4)^{1/2}}, \tag{23}$$

$$B^2 = 1 - \frac{F}{GC_{L0}^2 (S_G + \alpha)} \frac{\delta}{\delta^2 + 4}, \tag{24}$$

$$\varphi = \arctan\left(-\frac{2}{\delta} \right), \tag{25}$$

where δ must satisfy the cubic equation

$$\delta^3 - \Delta\delta^2 + 4\delta - 4\left[\Delta - \frac{F}{2\mu(S_G + \alpha)^2} \right] = 0. \tag{26}$$

In these equations, the detunings δ and Δ are defined by

$$\delta = \frac{2}{\mu(S_G + \alpha)} \left(\frac{\omega}{\omega_{n,i}} - 1 \right), \tag{27}$$

$$\Delta = \frac{2}{\mu(S_G + \alpha)} \left(\frac{\omega_S}{\omega_{n,i}} - 1 \right), \tag{28}$$

and the response parameter, or reduced damping, S_G is given by

$$S_G = \frac{\zeta_i}{\mu}. \tag{29}$$

Details of the perturbation/harmonic balance procedure involved in deriving equations (23)–(29) can be found in Skop & Griffin (1973) or in most treatises on nonlinear dynamics [see, for example, Minorsky (1962) or Nayfeh & Mook (1979)].

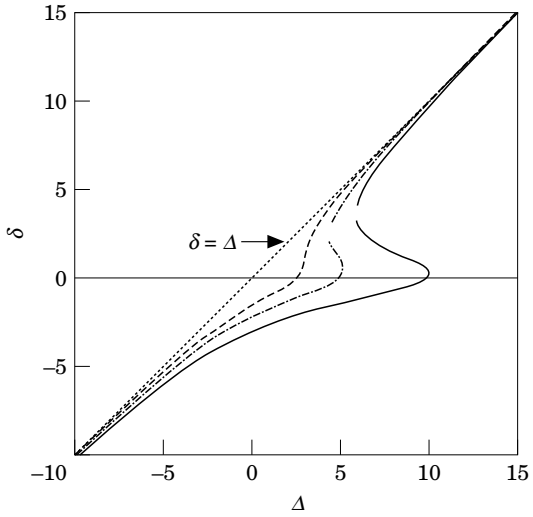

Figure 1. Behavior of the entrainment detuning δ versus the frequency detuning Δ for various values of the parameter $F/[2\mu(S_G+\alpha)^2]$: - - -, 2·5; - · -, 5·0; —, 10.

Equations (23)–(26) are known to yield accurate representations for the amplitudes A and B, the phase φ and the detuning δ throughout the resonant entrainment region upon the proper selection of the empirical parameters (Skop & Griffin 1973; Iwan & Blevins 1974). The starting point for this selection is equation (26), which determines the entrainment detuning δ, or equivalently the entrainment frequency ω, in terms of the frequency detuning Δ; or, equivalently, in terms of the Strouhal frequency ω_S or the flow speed V through equation (5). The δ versus Δ solution curves for various values of the parameter $F/[2\mu(S_G+\alpha)^2]$ are shown in Figure 1. For small values of this parameter, the solution curve for δ is a single-valued function of Δ. For larger values of $F/[2\mu(S_G+\alpha)^2]$, the solution curve for δ is multivalued over a range of Δ values and single valued outside of this range. In circumstances where a single solution exists for δ, Skop & Griffin (1973) and Ivan & Blevins (1974) have demonstrated that the solution corresponds to a physically realizable, or stable, solution to equations (17) and (18). In circumstances where three solutions exist for δ, Skop & Griffin (1973) and Iwan & Blevins (1974) have demonstrated that only the lower branch of the solution curve corresponds to a physically realizable solution to equations (17) and (18).

On introducing the factor Z, defined by

$$Z = \frac{F}{GC_{L0}^2(S_G+\alpha)}, \tag{30}$$

into equation (24), the excitation response amplitude B becomes

$$B^2 = 1 - \frac{Z\delta}{\delta^2+4}. \tag{31}$$

In turn, the structural response amplitude A becomes, from equations (23) and (31),

$$A^2 = \frac{C_{L0}^2}{(S_G+\alpha)^2}\frac{1}{\delta^2+4}\left(1-\frac{Z\delta}{\delta^2+4}\right). \tag{32}$$

The typical behavior of B and A as a function of Δ (that is, as a function of ω_S or V) can be ascertained from the above equations since, from Figure 1, δ is a monotonically increasing function of Δ in the stable entrainment region. That is, the behavior of B and A versus Δ is essentially the same as that of B and A versus δ, except for the numerical values assigned to the abscissa.

Consider this behavior. From equations (31) and (32), the derivatives of B^2 and A^2 with respect to δ are calculated, respectively, as

$$\frac{dB^2}{d\delta} = \frac{Z(\delta^2 - 4)}{(\delta^2 + 4)^2}, \tag{33}$$

$$\frac{dA^2}{d\delta} = \frac{C_{L0}^2}{(S_G + \alpha)^2}\left[\frac{-2\delta^3 + 3Z\delta^2 - 8\delta - 4Z}{(\delta^2 + 4)^3}\right]. \tag{34}$$

Thus, the maximum of B, $B_{\max}$, occurs at $\delta = -2$ and has there, from equation (31), the value $B_{\max} = (1 + Z/4)^{1/2}$. Also, at $\delta = -\sqrt{4/3}$, we have $dA^2/d\delta > 0$ and, at $\delta = 0$, $dA^2/d\delta < 0$. Hence, the peak value of A occurs between $\delta = -\sqrt{4/3}$ and $\delta = 0$.

The variation of B and A versus δ is sketched in Figure 2. On recalling that this is equivalent to the behavior versus Δ, a qualitative resemblance with experimental observations [as shown, for example, in Skop & Griffin (1973)] is apparent. In particular, both the excitation response amplitude and the structural displacement undergo resonant type amplifications in the stable entrainment region; and, also, the peak value of the excitation response amplitude leads the peak value of the structural displacement. It remains to quantify this qualitative agreement.

Let δ_A denote the value of δ at which the maximum value of A, $A_{\max}$, occurs. Here, δ_A is not an experimentally determined quantity, but rather must be selected so that the predicted $A_{\max}$ agrees with the observed $A_{\max}$. From equation (34), when $A = A_{\max}$, the condition

$$Z = \frac{2\delta_A(\delta_A^2 + 4)}{3\delta_A^2 - 4} \tag{35}$$

must hold. When this condition is substituted into equation (32), a bi-quadratic

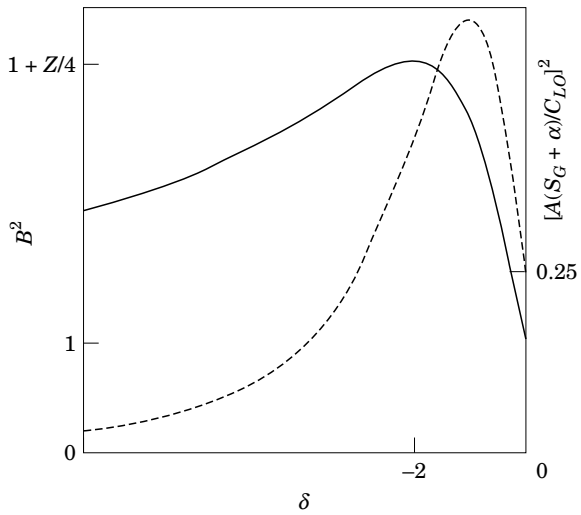

Figure 2. Typical behavior of the excitation response amplitude B and the structural response amplitude A versus the entrainment detuning δ.

equation for δ_A, with coefficients in terms of $A_{\max}$, results. The solution to the bi-quadratic equation provides the required value of δ_A as

$$\delta_A = -\left\{\frac{-(8X-1)+\sqrt{(8X-1)^2+48X(4X-1)}}{6X}\right\}^{1/2}, \tag{36}$$

where the quantity X is defined by

$$X = \left[\frac{(S_G+\alpha)A_{\max}}{C_{L0}}\right]^2. \tag{37}$$

For equation (36) to hold, the constraint $X \geq 1/4$ is needed to ensure non-negativeness of the term within the braces. Equivalently, the proviso,

$$\alpha \geq \frac{C_{L0}}{2A_{\max}} - S_G, \tag{38}$$

must be satisfied. The empirical parameter G can now be obtained in terms of the empirical parameter F by substituting equation (35) for Z into equation (30). Specifically, G is found as

$$G = \frac{F}{2C_{L0}^2(S_G+\alpha)}\frac{3\delta_A^2-4}{\delta_A(\delta_A^2+4)}. \tag{39}$$

Let us, additionally, denote by Δ_A the experimentally observed frequency detuning Δ at which $A_{\max}$ occurs. From equation (28), Δ_A is defined by

$$\Delta_A = \frac{2}{\mu(S_G+\alpha)}\left(\frac{\omega_{S,A}}{\omega_{n,i}}-1\right), \tag{40}$$

where $\omega_{S,A}$ denotes the inherent vortex-shedding frequency when $A = A_{\max}$. For δ_A to occur simultaneously with Δ_A requires that equation (26) for δ has a solution when $\delta = \delta_A$ and $\Delta = \Delta_A$. This requirement then provides the empirical parameter F as

$$F = \frac{\mu(S_G+\alpha)^2}{2}(\delta_A^2+4)(\Delta_A-\delta_A). \tag{41}$$

To evaluate δ_A and Δ_A from equations (36) and (40), respectively, entails obtaining experimental measurements of $A_{\max}$ and $\omega_{S,A}/\omega_{n,i}$ as functions of the response parameter S_G. It is useful to recall, from equations (19) and (21), that $A_{\max}$ is related to the actual experimental measurements of the structural displacement $Y(x, t)$ through the modal normalization,

$$A_{\max} = \frac{Y_{\max}(x,t)}{\Gamma_i^{1/2}\psi_{i,\max}(x)}. \tag{42}$$

The available data for circular cylindrical structures is summarized in the Appendix. The values of S_G and $A_{\max}$ given in the Appendix have been tabulated by Griffin (1994) and, for the most part, also appear elsewhere [see, for example, Griffin *et al.* (1982)]. For the experiments in water, however, we have gone to the original source material

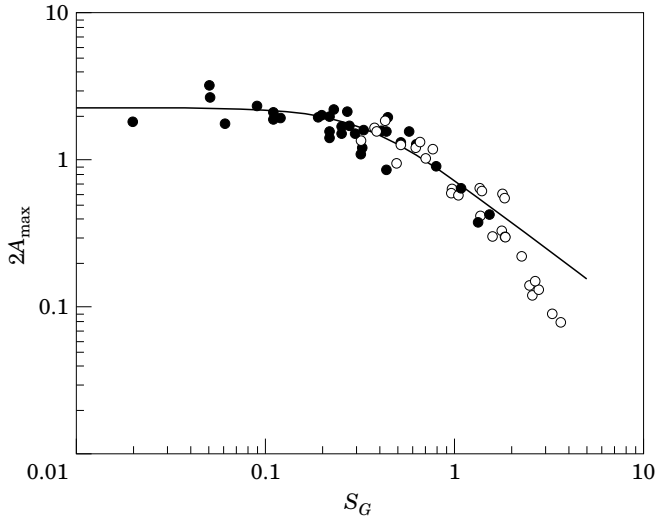

Figure 3. Experimental measurements of the modally normalized, maximum structural response amplitude $A_{\max}$ versus the response parameter S_G. The data plotted is summarized in the Appendix. ○, In-air measurements; ●, in-water measurements; —, semi-empirical, least-squares fit to the data, given by equation (43).

to determine the corrected values of ζ_i from equation (3) and, hence, the appropriate values of S_G from equation (29). The values of $\omega_{S,A}/\omega_{n,i}$ have been ascertained from the original source material.

The data points for $A_{\max}$ are plotted versus S_G in Figure 3. A least-squares fit to the data points, given by

$$A_{\max} = \frac{0{\cdot}385}{(0{\cdot}12 + S_G^2)^{1/2}}, \tag{43}$$

is also plotted in the figure. The permissible functional form of the least-squares fit was arrived at by Sarpkaya (1978) based on a semi-empirical analysis of vortex-excited vibrations. We have, however, recalculated his original constants to reflect the more extensive data set summarized in the Appendix. The semi-empirical fit slightly overpredicts the small amplitudes of vibration at larger values of S_G. This overprediction is expected since, as noted by Sarpkaya, the semi-empirical fit assumes phase-locked vortex shedding along the entire cylinder. This phase-locked vortex shedding does not occur at low amplitudes of vibration. The data points for $\omega_{S,A}/\omega_{n,i}$ are plotted versus S_G in Figure 4. There is some scatter in the data points, but with a trend towards higher values of $\omega_{S,A}/\omega_{n,i}$ for the in-water experiments as compared to the in-air experiments. The mean value of the data points for the in-water experiments is 1·30, while the mean value for the in-air experiments is 1·216. The in-water experiments also tend to be at lower values of S_G than the in-air experiments. To reflect these trends, we have fitted the data with a doubly asymptotic, least-squares fit given by

$$\frac{\omega_{S,A}}{\omega_{n,i}} = 1{\cdot}216 + \frac{0{\cdot}084}{1 + 2{\cdot}66S_G^2}. \tag{44}$$

The curve defined by equation (44) is also plotted in Figure 4.

The substitution of equations (43) and (44) into equations (36) and (40) uniquely determines δ_A and Δ_A in terms of the material properties of the structure, once C_{L0}, S and α are specified. In turn, the empirical parameters G and F, from equations (39)

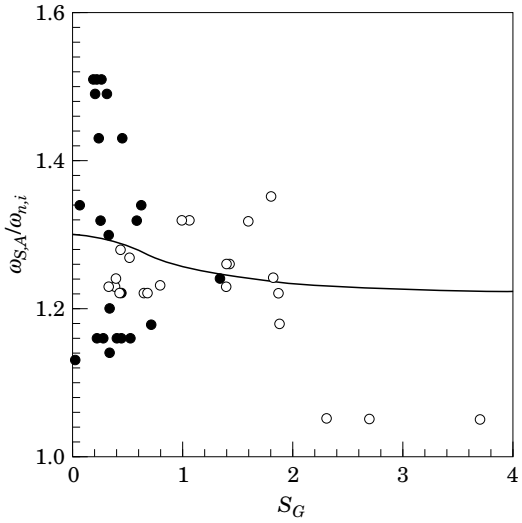

Figure 4. Experimental measurements of the frequency ratio $\omega_{S,A}/\omega_{n,i}$ at which $A_{\max}$ occurs versus the response parameter S_G. The data plotted is summarized in the Appendix. ○, In-air measurements; ●, in -water measurements; —, doubly asymptotic, least-squares fit to the data, given by equation (44).

and (41), respectively, are also uniquely determined in terms of the material properties of the structure, once C_{L0}, S and α are specified. For a circular section, the value for C_{L0} is taken as $C_{L0} = 0{\cdot}28$ as quoted by Protos *et al.* (1968). The value of S is taken as $S = 0{\cdot}21$, which is appropriate to the subcritical range, approximately from 3×10^2 to 3×10^5, of Reynolds number. The stall parameter α must still be evaluated. However, the constraint on this parameter imposed by equation (38) can be restated. Simple numerical calculations, using equation (43) in equation (38), show that the right-hand side of equation (38) is a monotonically decreasing function of S_G. Hence, the constraint on α becomes

$$\alpha \geq \frac{C_{L0}}{2A_{\max,0}} = 0{\cdot}126, \tag{45}$$

where $A_{\max,0}$ represents the value of $A_{\max}$ at $S_G = 0$ and, from equation (43), is given by $A_{\max,0} = 1{\cdot}11$.

The fact that G and F depend on the material properties of the structure, instead of being universal constants, is the price one must accept for reducing a complex fluid–structural interaction problem to a leading-order approximation. The situation is similar to that encountered in low order modeling of turbulent flows where the modeling parameters must be adjusted for the geometry of the flow boundaries [see, for example, Rodi (1980)].

4. MECHANICALLY OSCILLATED CYLINDERS AND THE STALL PARAMETER

Let us now turn our attention to a rigid cylinder which is mechanically oscillated in a direction transverse to the incoming cross-flow. In this case, the structural mass and damping of the cylinder have no influence on the vortex-shedding process and can be set to zero. However, the acceleration of the mechanically oscillated cylinder still provides feedback to the fluid through the added mass term m_a. Hence, for a

mechanically oscillated cylinder, we have $m_S = 0$ and $\zeta_i = 0$, but $m_a \neq 0$. We also have, from equations (12) and (29) for μ and S_G, respectively, that $\mu \neq 0$ while $S_G = 0$.

For a circular section, the added mass coefficient is unity and the added mass is given by $m_a = \pi\rho D^2/4$. The mass ratio parameter, μ, for a mechanically oscillated cylinder then reduces to

$$\mu = \frac{1}{2\pi^3 S^2} = 0{\cdot}366. \tag{46}$$

The quantity X defined by equation (37) and used to calculate δ_A from equation (36) becomes

$$X = \left(\frac{\alpha A_{\max,0}}{C_{L0}}\right)^2 = 15{\cdot}76\alpha^2. \tag{47}$$

Additionally, the frequency detuning Δ_A defined by equation (40) is found as

$$\Delta_A = \frac{1{\cdot}641}{\alpha} \tag{48}$$

on substituting for $\omega_{S,A}/\omega_{n,i}$ from equation (44) and for μ from equation (46). In Consequently, for a mechanically oscillated cylinder, the empirical parameters G and F, given by equations (39) and (41), respectively, are all implicit functions of the stall parameter α alone.

The normalized displacement of the rigid cylinder is defined by

$$Y(x, t) = A \sin \omega_f t, \tag{49}$$

where A and ω_f are, respectively, the mechanically imposed amplitude and frequency of the oscillation. Under the condition $\omega_S \approx \omega_f$, we seek the synchronized solution to equation (6) for the excitation component of the fluctuating lift coefficient as

$$Q(x, t) = BC_{L0} \sin(\omega_f t + \varphi). \tag{50}$$

Here, B is the amplification factor for the excitation component of the fluctuating lift coefficient and φ is the phase of this component relative to the mechanically oscillated cylinder. On substituting equations (49) and (50) into equation (6), the amplification factor for the synchronized response is found to satisfy the bi-cubic equation,

$$G^2B^6 - 2G^2B^4 + (G^2 + \delta_f^2)B^2 - \left(\frac{FA}{C_{L0}^3}\right)^2 = 0, \tag{51}$$

while the phase is given by

$$\varphi = \arctan\left[\frac{\delta_f}{G(B^2 - 1)}\right]. \tag{52}$$

In these equations, the detuning δ_f is defined by

$$\delta_f = \frac{2}{C_{L0}^2}\left(\frac{\omega_s}{\omega_f} - 1\right). \tag{53}$$

For a solution to equation (51) to be physically realizable, it must satisfy simultaneously the two conditions:

$$2B^2 - 1 \geq 0, \tag{54}$$

$$G^2(B^2 - 1)(3B^2 - 1) + \delta_f^2 \geq 0. \tag{55}$$

Again, details of the procedure involved in deriving equations (51)–(55) can be found in Skop & Griffin (1973) or in treatises on nonlinear dynamics, such as Minorsky (1962) or Nayfeh & Mook (1979).

The boundary of equation (55) is an ellipsoid in the $\delta_f - B$ plane and the stable solutions to equation (41) are those which lie outside of this ellipsoid and above $B = 1/\sqrt{2}$. The value of B along the boundary of equation (55) is given in terms of δ_f by

$$B = \left(\frac{2G \pm \sqrt{G^2 - 3\delta_f^2}}{3G}\right)^{1/2}. \tag{56}$$

The boundary between the stable and unstable solutions of equation (51) is plotted schematically in Figure 5. Some stable solutions to equation (51), with increasing driving amplitude A, are also plotted in the figure. The values of δ_f at the left and right vertical tangents to the stability ellipsoid are determined by the vanishing of the interior radical in equation (56); from which, we find $\delta_f = \pm G/\sqrt{3}$. The value of the amplification factor B at the left and right vertical tangents follows from equation (56) as $B = \sqrt{2/3}$. The driving amplitude A which produces the value of B at a vertical tangent occurring at δ_f is then found directly from equation (51) as

$$A = \left(\frac{2}{3}\right)^{3/2} \frac{GC_{L0}^3}{F}. \tag{57}$$

The value of the driving amplitude at the left and right vertical tangents is shown versus the stall parameter α in Figure 6. For values of α greater than approximately 0·18, the solution curves to equation (51) intersect the stability ellipsoid only for small values of A, as is apparent from Figure 6. For example, for $\alpha = 0{\cdot}18$, only solution curves for $A \leq 0{\cdot}10$ intersect the stability ellipsoid. Consequently, except for small values of the driving amplitude, the boundaries of the δ_f space for which a stable, synchronized solution for Q exists can be determined by setting $B = 1/\sqrt{2}$ in equation (51).

The synchronization boundaries are shown for various values of α in Figure 7. The ordinate in this figure has been converted from δ_f to $\omega_S/\omega_f - 1$ through equation (53). The gaps in the curves correspond to values of A for which stability is determined by

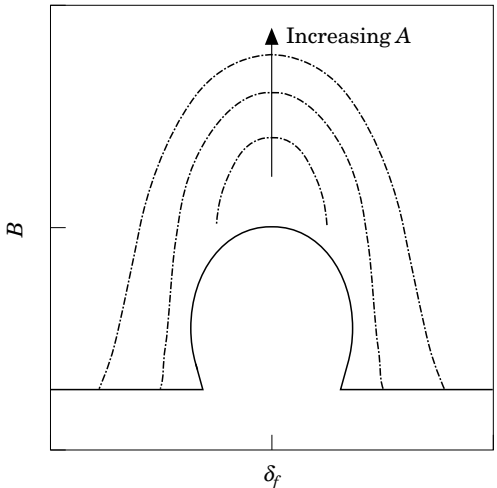

Figure 5. Schematic plot of the boundary between stable and unstable values of the amplification factor B versus the driving detuning δ_f. Some stable solutions for B versus δ_f, as a function of increasing driving amplitude A, are also shown.

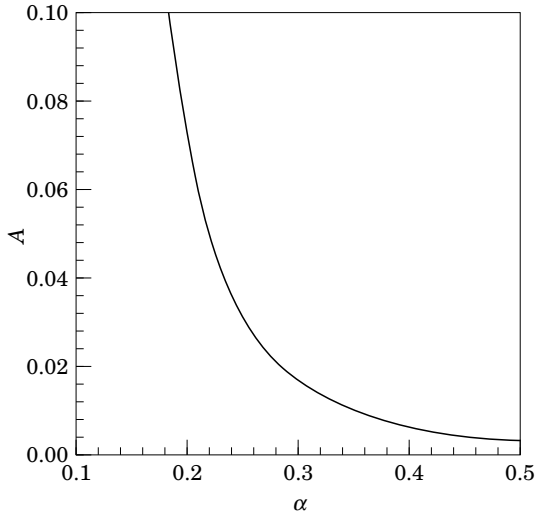

Figure 6. The driving amplitude A at the left and right vertical tangents to the stability ellipsoid versus the stall parameter α.

the stability ellipsoid rather than by $B = 1/\sqrt{2}$. The boundaries of the synchronization region found experimentally by Williamson & Roshko (1988) are also shown in Figure 7. Generally, the predicted synchronization boundaries for values of α between 0·17 and 0·19 provide somewhat reasonable agreement to the experimentally measured synchronization boundaries. However, the experimentally determined boundaries are asymmetric about $\omega_S/\omega_f - 1 = 0$, while the predicted boundaries are symmetric.

The width of the synchronization region—that is, the distance between the lower and upper synchronization boundaries—versus the driving amplitude A is shown for various values of α in Figure 8. The width of the synchronization region found experimentally

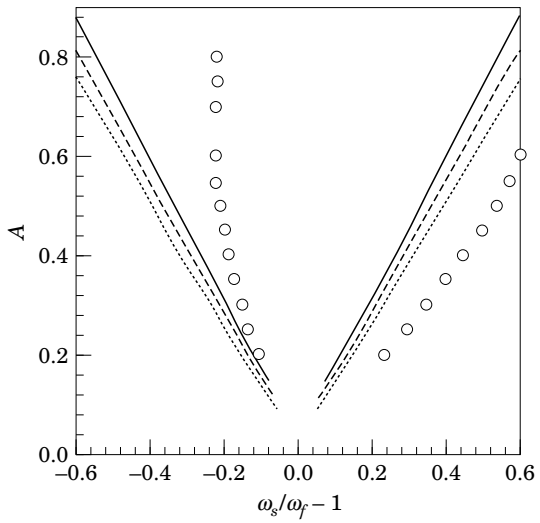

Figure 7. The boundaries between which a stable, synchronized solution for Q exists as a function of the driving amplitude A and the driving detuning $\omega_S/\omega_f - 1$. The boundaries are shown for values of the stall parameter α: —, $\alpha = 0{\cdot}17$; - - -, $\alpha = 0{\cdot}18$; · · · ·, $\alpha = 0{\cdot}19$. The open circles are the boundaries experimentally determined by Williamson & Roshko (1988).

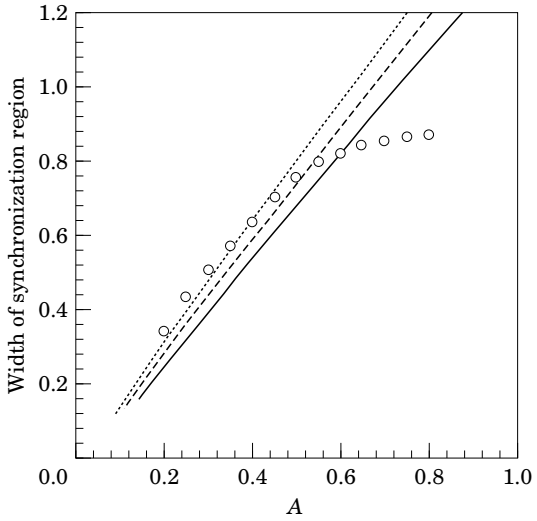

Figure 8. The width of the synchronization region as a function of the driving amplitude A. The width is shown for three values of the stall parameter α: —, $\alpha = 0{\cdot}17$; - - -, $\alpha = 0{\cdot}18$; . . . , $\alpha = 0{\cdot}19$. The open circles are the widths experimentally determined by Williamson & Rushko (1988).

by Williamson & Roshko (1988) is also shown in this figure. The predicted and measured widths are in good agreement for values of α between 0·17 and 0·19 and for values of A less than about 0·60.

A value of 0·183 for α gives a value of 0·20 for GC_{L0}^2 for modeling vortex shedding from a mechanically oscillated cylinder. Interestingly, this value of GC_{L0}^2 has been used by Noack *et al.* (1991) and by us (Skop & Balasubramanian 1995*b,* Balasubramanian & Skop 1996) in connection with a diffusive van der Pol equation for modeling vortex shedding from cylinders in nonuniform flow fields. For consistency among models, the value of α is, hence, taken as $\alpha = 0{\cdot}183$. This value for α, together with equations (39) and (41) for calculating G and F, respectively, given the system values for the mass ratio μ and response parameter S_G, completes the specification of the empirical parameters.

5. CONCLUSIONS

A modification to a previous model for predicting vortex-excited vibrations of flexible cylindrical structures has been developed. The modification consists of incorporating a stall term as one component of the fluctuating lift force on the cylinder. The other component of the lift force is governed by a van der Pol equation which itself is driven by the motion of the cylinder.

The methodology by which the empirical parameters appearing in the model have been evaluated, so that the model predictions agree with experimental measurements, has been described in detail. This methodology is appropriate to cylinders having noncircular cross-sections given sufficient experimental or numerical response measurements. These measurements can be obtained for the simple case of a spring-mounted cylinder. The model can then be used to predict the responses of more complex flexible cylindrical structures having the same cross-section.

In the course of the model development, several issues which have arisen over the years in discussions of nonlinear oscillator models for describing vortex-excited vibrations have been addressed. One issue concerned the proper value of the in-water

structural damping coefficients to be used in the models. This issue is resolved by equation (3). A second issue concerned the form of the feedback of the structural motion to the nonlinear oscillators. By consideration of the experimentally verified, modal scaling principle, we have demonstrated that the form of the feedback must be either linear or cubic in the model variables. We have used the linear form in this paper since it is consistent with the leading order nature of the nonlinear oscillator models.

ACKNOWLEDGMENTS

The work reported here has been sponsored by the U.S. Office of Naval Research under grant N00014-93-1-0438. The authors gratefully acknowledge this support. *The senior author* (*RAS*) *would like to dedicate this paper to the memory of Owen M. Griffin, with whom he developed the* ''*Old Model*'' *alluded to in the title.*

REFERENCES

ALBARÈDE, P. & MONKEWITZ, P. A. 1992 A model for the formation of oblique shedding and ''Chevron'' patterns in cylinder wakes. *Physics of Fluids A* **4,** 744–756.

BALASUBRAMANIAN, S. & SKOP, R. A. 1996 A nonlinear oscillator model for vortex shedding from cylinders and cones in uniform and shear flows. *Journal of Fluids and Structures* **10,** 197–214.

BILLAH, K. Y. R. 1989 A study of vortex-induced vibrations. Ph.D. Dissertation, Princeton University, Princeton, NJ, U.S.A.

GRIFFIN, O. M. 1994 Private communication.

GRIFFIN, O. M., VANDIVER, J. K., SKOP, R. A. & MEGGITT, D. J. 1982 The strumming vibrations of marine cables. *Ocean Science and Engineering* **7,** 461–498.

HARTLEN, R. & CURRIE, I. 1970 Lift-oscillator model for vortex-induced vibrations. *ASCE Journal of Engineering Mechanics* **96,** 577–591.

IWAN, W. D. 1975 The vortex induced oscillation of elastic structural elements. *ASME Journal of Engineering for Industry* **97,** 1378–1382.

IWAN, W. D. & BLEVINS, R. D. 1974 A model for vortex induced oscillation of structures. *Journal of Applied Mechanics* **41,** 581–586.

MINORSKY, N. 1962 *Nonlinear Oscillations.* Princeton, NJ: D. Van Nostrand.

NAYFEH, A. H. & MOOK, D. T. 1979. *Nonlinear Oscillations.* New York: John Wiley & Sons.

NOACK, B. R., OHLE, F. & ECKELMANN, H. 1991 On cell formation in vortex streets. *Journal of Fluid Mechanics* **227,** 293–308.

PARKINSON, G. 1989 Phenomena and modelling of flow-induced vibrations of bluff bodies. *Progress in Aerospace Science* **26,** 169–224.

PROTOS, A., GOLDSCHMIDT, V. & TOEBES, G. 1968 Hydroelastic forces on bluff cylinders. *ASME Journal of Basic Engineering* **90,** 378–386.

RAMBERG, S. E. & GRIFFIN, O. M. 1974 Vortex formation in the wake of a vibrating, flexible cable. *ASME Journal of Fluids Engineering* **96,** 317–322.

RAMBERG, S. E. & GRIFFIN, O. M. 1976 Velocity correlation and vortex spacing in the wake of a vibrating cable. *ASME Journal of Fluids Engineering* **98,** 10–18.

RODI, W. 1980. *Turbulence Models and their Application in Hydraulics.* Delft, The Netherlands: International Association for Hydraulic Research.

SARPKAYA, T. 1978 Fluid forces on oscillating cylinders. *ASCE Journal of Waterway, Port, Coastal and Ocean Engineering* **104,** 275–290.

SKOP, R. A. & BALASUBRAMANIAN, S. 1995*a* A nonlinear oscillator model for vortex shedding from a forced cylinder. Part 1: Uniform flow and model parameters. *International Journal of Offshore and Polar Engineering* **5,** 251–255.

SKOP, R. A. & BALASUBRAMANIAN, S. 1995*b* A nonlinear oscillator model for vortex shedding from a forced cylinder. Part 2: Shear flow and axial diffusion. *International Journal of Offshore and Polar Engineering* **5,** 256–260.

SKOP, R. A. & GRIFFIN, O. M. 1973 A model for the vortex-excited resonant response of bluff cylinders. *Journal of Sound and Vibration* **27,** 225–233.

SKOP, R. A. & GRIFFIN, O. M. 1975 On a theory for the vortex-excited oscillations of flexible cylindrical structures. *Journal of Sound and Vibration* **41,** 263–274.

THOMSON, W. T. 1965 *Vibration Theory and Applications.* Englewood Cliffs, NJ: Prentice-Hall.

TRIANTAFYLLOU, M. S., GOPALKRISHNAN, R. & GROSENBAUGH, M. A. 1994 Vortex-induced vibrations in a sheared flow: a new predictive method. In *Hydroelasticity in Marine Technology* (eds Faltinsen *et al.*), pp. 31–37. Rotterdam: Balkema.

WILLIAMSON, C. H. K. & ROSHKO, A. 1988. Vortex formation in the wake of an oscillating cylinder. *Journal of Fluids and Structures* **2,** 355–381.

APPENDIX

Source	Fluid	Type†	S_G	$2A_{\max}$	$\omega_{S,A}/\omega_{n,i}$††
a	water	P	0·09	2·30	na
			0·11	2·10	na
			0·12	1·90	na
			0·22	1·40	na
			0·25	1·50	na
			0·80	0·92	na
			1·18	0·66	na
			1·56	0·43	na
			1·90	0·30	na
	air		1·80	0·33	na
b	air	C	2·30	0·22	1·05
			2·70	0·15	1·05
			3·70	0·08	1·05
c	water	Ca-4	0·22	1·56	1·16
		Ca-3	0·33	1·23	1·20
		Ca-2	0·44	0·87	1·22
d	air	S	0·32	1·36	1·23
			0·38	1·64	1·23
			0·39	1·57	1·24
			0·43	1·84	1·28
			0·52	1·25	1·22
			0·63	1·20	1·22
			0·66	1·32	1·22
			0·78	1·20	1·23
			1·37	0·65	1·23
			1·41	0·62	1·26
			1·82	0·60	1·24
			1·86	0·56	1·22
e	air	S	0·98	0·64	na
f	air	P	2·50	0·14	na
			2·60	0·12	na
			2·80	0·13	na
			3·30	0·09	na
g	air	S	0·72	1·04	na
			0·97	0·60	1·32
			1·39	0·42	1·26
			1·87	0·30	1·18
h	air	S	1·90	0·30	na
i	air	S	0·50	0·96	1·27
			1·05	0·58	1·32
			1·60	0·30	na
j	water	S	0·32	1·10	1·14

APPENDIX—(*Continued*)

Source	Fluid	Type†	S_G	$2A_{\max}$	$\omega_{S,A}/\omega_{n,i}$††
k	water	C	0·05	3·20	na
			0·05	2·60	na
			0·11	1·85	na
			0·19	1·94	1·51
			0·20	2·00	1·49
			0·22	1·90	1·51
			0·27	2·10	1·51
			0·30	1·50	1·49
			0·45	1·95	1·43
			1·34	0·38	1·24
l	water	S	0·02	1·86	1·13
			0·06	1·75	1·34
			0·25	1·68	1·32
			0·28	1·70	1·16
			0·33	1·59	1·30
			0·40	1·60	1·16
			0·44	1·56	1·16
			0·52	1·30	1·16
			0·58	1·55	1·32
			0·63	1·30	1·34
			0·71	1·02	1·18
m	water	S	0·23	2·18	1·43

† S = spring-mounted cylinder; P = pivoted cylinder; C = cantilevered cylinder, first mode; Ca-i = taut cable, *i*th mode

†† na = not available

a. Vickery, B. J. & Watkins, R. D. 1964 Flow-induced vibrations of cylindrical structures. In *Proceedings of the First Australian Conference on Hydraulics and Fluid Mechanics* (ed. R. Silvester), New York: Pergamon Press.

b. Scruton, C. 1963 On the wind-excited oscillations of towers, stacks and masts. In *Proceedings of the Symposium on Wind Effects on Structures,* Teddington, U.K.

c. Dale, J. R., Menzel, H. & McCandless, J. 1966 Dynamic characteristics of wire rope: flow-induced cable vibrations. U.S. Naval Air Development Center Report NADC-AE-6620, Warminster, PA. (Note: The values of S_G were subsequently determined in *n.*)

d. Glass, R. J. 1966 A study of the self-excited vibrations of spring-supported cylinders in a steady stream. Ph.D. Dissertation University of Maryland, College Park, MD, U.S.A.

e. Ferguson, N. & Parkinson, G. 1967 Surface and wake phenomena of vortex-excited oscillations of bluff cylinders. *ASME Journal of Engineering for Industry* **89,** 831–838.

f. Hartlen, R., Baines, W. & Currie, I. 1968. Vortex-excited oscillations of a circular cylinder. University of Toronto Technical Publication 6809, Toronto, Canada.

g. Parkinson, G., Feng, C. & Ferguson, N. 1968 Mechanisms of vortex-excited oscillations of bluff cylinders. In *Proceedings of the Symposium on Wind Effects on Buildings and Structures,* Loughborough, U.K.

h. Koopmann, G. H. 1970 Wind-induced vibrations of skewed circular cylinders. Civil and Mechanical Engineering Department Report 70–11, Catholic University of America, Washington, DC.

i. Griffin, O. M., Skop, R. A. & Koopmann, G. H. 1973 The vortex-excited resonant vibrations of circular cylinders. *Journal of Sound and Vibration* **31,** 235–249.

j. Angrilli, F., DiSilvio, G. & Zanardo, A. 1974 Hydroelasticity experiments on circular cylinder in water stream. In *Proceedings of the IUTAM-IAHR Symposium on Flow-Induced Structural Vibrations,* Berlin: Springer-Verlag.

k. King, R. 1974 Vortex-excited structural oscillations of a circular cylinder in flowing water. Doctoral Thesis, Loughborough University of Technology, Loughborough, U.K.

l. Dean, R. B., Milligan, R. W. & Wootton, L. R. 1977 Study of flow-induced vibration. Atkins Research and Development Report, London.

m. Moe, G. & Overvik, T. 1982 Current-induced motions of multiple risers. In *Proceedings of BOSS-82, Behavior of Offshore Structures,* Vol. 1, Cambridge, MA, U.S.A.

n. Ramberg, S. E. & Griffin, O. M. 1974 Some transverse resonant vibration characteristics of wire rope with application to flow-induced cable vibrations. U.S. Naval Research Laboratory Formal Report 7821, Washington, DC, U.S.A.